Geomorphic and Geophysical Studies from the Sukri River Watersheds, Rajasthan, India

Adrija Raha, Kutubuddin Ansari, and Soumyajit Mukherjee

Abstract Two morphometric approaches are applied on the Sukri River's watersheds to study their tectonic activeness. Based on Analytic Hierarchic Process (AHP) and Index of Active Tectonics (IAT) studies, sub-watershed 1 (SW1) and 2 delineated are highly active tectonically, SW6 and 7 are moderately active, and SW5 shows a low tectonic activeness. Both approaches reaching common results confirm the morphological findings of this study. Bathymetry (topographic) and gravity variation in the Sukri basin are studied. The results clearly show a height variation within 200–1600 m, with a 1400 m upward continuation and no specific elevation trend. Several depressions can be seen within the region because of the available graben. The gravity contour plot in the Sukri basin also shows no particular trend similar to the topographic map. The gravity values within the region vary from − 10 to 80 mGal. The difference between high and low gravity anomalies is ~ 90 mGal could be possible because of grabens. We also estimated bathymetry gravity, which is a function of bathymetry and estimated their percentage deviation (PD). The obtained result of PD shows its deviation varies from -400 to 1200% within the region.

Keywords Neotectonics · Active tectonics · Geomorphological analyses · Tectonics · Gravity · Bathymetry · Percentage deviation

A. Raha
Department of Geography, Presidency University, Kolkata, West Bengal, India

K. Ansari
Integrated Geoinformation (IntGeo) Solution Private Limited, New Delhi, India

S. Mukherjee (✉)
Department of Earth Sciences, Indian Institute of Technology Bombay, Powai, Mumbai, Maharashtra, India
e-mail: smukherjee@iitb.ac.in; soumyajitm@gmail.com

S. Mukherjee and N. R. Kar (eds.), *Geosciences of the Rajasthan Basins, India*, Springer Geology, https://doi.org/10.1007/978-981-96-3005-9_9

1 Introduction

1.1 Geomorphic Approaches

Industrial and academic experts have been investigating the Rajasthan basins (e.g. Dasgupta and Mukherjee 2017; Biswas et al. 2022a, b; Kar et al. 2022; Puniya et al. 2023a, b; Biswas et al. 2024).

Active tectonics studies the dynamic processes influencing the formation of the landforms and their changes (Yemani et al. 2011). In particular, active tectonics is studied using geomorphic indices (Goorabi and Nohegar 2005). Rivers are studied to assess active tectonics since they are one of the most significant landscapes on Earth and are sensitive to tectonic activity. Many geological and hydrological processes alter river's course. This is followed by morphological changes and bank erosion (Telvari 2009; Yargholi and Goraji 2014).

Because the landscape retains a significant archive of the rates and spatial distribution of deformation, geomorphology plays key role in the study of active fault systems (Kirby and Whipple 2012). Active tectonism has been extensively studied through the use of geomorphic indices, which are able to identify landform responses to deformation processes (e.g. Brookfield 1998; Keller and Printer 2002; Chen 2003; El Hamdouni et al. 2008; Gao et al. 2013).

Understanding the processes of landform development, soil physical qualities and erosion characteristics depends critically on the efficacy of the drainage network morphometric (Malik et al. 2011; Okumura and Araujo 2014; Rodrigo-Comino et al. 2016). A number of studies have already utilised the Index of Active Tectonics (IAT) to rank the watersheds according to tectonic activity (Anand and Pradhan 2019).

In this work, the sub-watersheds' reaction to tectonic activity has been prioritised using both the Analytic Hierarchic Process (AHP) and IAT.

1.2 Geophysical Approaches

The gravity method for the detection of geological features and faults has been widely used in several parts of the globe (Nyalugwe et al. 2020; Yanis et al. 2020; Dewanto et al. 2022). The physical principle of gravity method is based on Newton's gravitation law, which states that the value of working force between two mass bodies is directly correlated to the multiplication of their masses and inversely correlated to the square of distance between them (Surya et al. 2019; Benyas et al. 2021). The gravity method is a type of geophysical method used to measure the difference between the gravity of the Earth and its density variation alongside each measurement (Yanis et al. 2023). The free-air gravity anomaly measurements are the values of gravity accelerations that are topography affected that do not consider the mass of rock in subsurface. Gravitational data interpretation and analysis are generally given by their horizontal

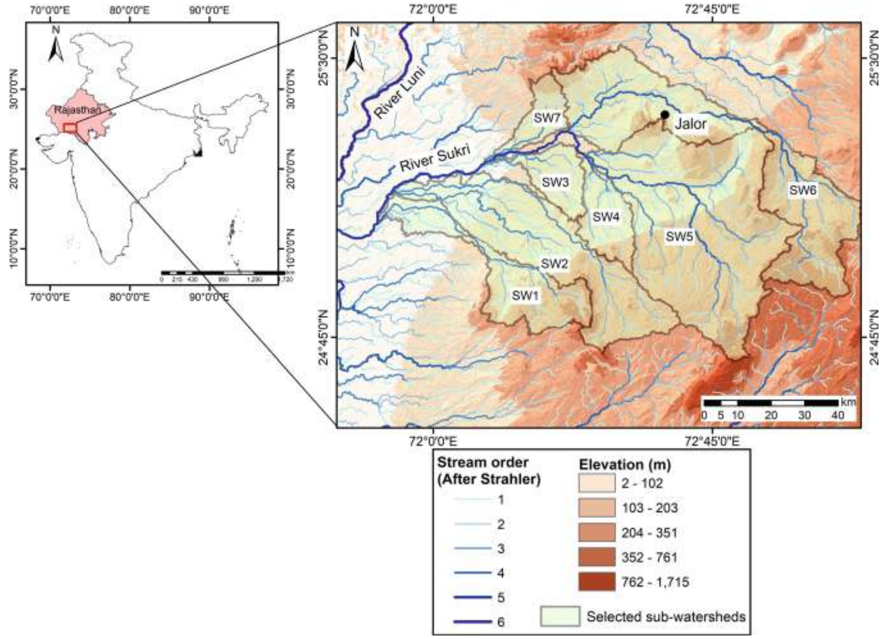

Fig. 1 Delineated sub-watersheds of river Sukri

and vertical derivative spatial variations. The current study presents an analysis of gravity in the Sukri basin and its direct relation with bathymetry (topography).

2 Study Area

The river Sukri, a left-hand tributary of the Luni River, has been chosen (Fig. 1). Sukri is a river of fifth order with seven major tributaries. The Sukri river basin is a part of the mid-west alluvial plain and is located west of the Aravalli range. Orographically, the basin's eastern section is characterised by hilly terraces of the Aravalli chain, while to the west of these hills lies a narrow alluvial plain that gradually slopes westward.

3 Geology and Tectonics

The Indian desert is an extension of the Peninsular region geologically. Undifferentiated Aeolian deposits from the Quaternary era cover the maximum area. The Neoproterozoic–Mesoproterozoic Erinpura Granite and Gneiss comprise the highest

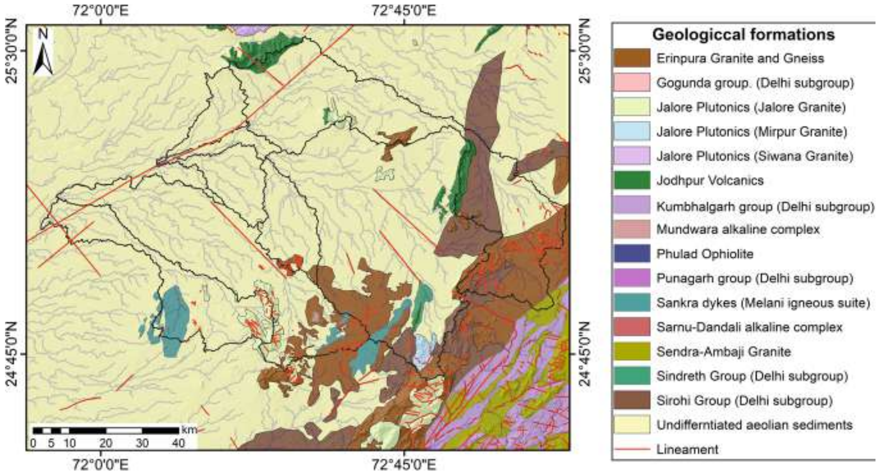

Fig. 2 Major geological formations and lineaments of the study area. *Source* https://bhukosh.gsi.gov.in

portions of the sub-watersheds. Jalore plutonic (granite) rocks are present in tiny places, particularly over the sub-watershed 1 (SW1) and SW2. Sankra Dykes /Malani Igneous suite is located at the far-right portion of SW1. A distinct NE-SW lineament that runs along the major Sukri River channel. On the sub-watersheds' catchment regions, several smaller lineaments are documented (Fig. 2).

4 Methodology

4.1 Morphometry

On the ArcGIS 10.4 platform, seven sub-watersheds of Sukri are identified. To extract the streams and sub-watersheds, a 30-m resolution Shuttle Radar Topographic Mission (SRTM) Digital Elevation Model is utilised. Six morphometric parameters were studied (Table 1). Tectonic activity is utilised to rank the sub-watersheds using the Analytic Hierarchical Process (AHP). The ArcGIS 10.4 platform generates raster files for every parameter. These are then categorised appropriately. The weights determined by AHP are applied using the weighted sum approach. Sub-watersheds have also been categorised according to tectonic activity using the Index of Active Tectonics (IAT).

Table 1 Selected morphometric parameters for the sub-watersheds

Formula for basin scale indicators	Equations and meaning of symbols	Explanations	References
Asymmetry factor (AF)	$AF = \left(\frac{A_r}{A_t}\right) * 100$ A_r: area of the basin (km^2) to the right of the main channel facing downstream and A_t: total area (km^2) of the basin	An indicator to measure how much a river basin is tilted under the influence of tectonics	Hare and Gardner (1985)
Transverse topographic symmetry (T)	$T = \frac{\mathrm{Da}}{\mathrm{Dd}}$ Da: the distance from the drainage basin's midline to the meander belt's midline Dd: the distance from the basin's midline to the basin divide	$T = 0$ for a symmetric basin. As asymmetry develops, T rises and eventually equals 1	Cox (1994)
Form factor (R_f)	$R_f = \frac{A}{L_b^2}$ A: signifies the area of the basin, L_b: denotes the length of the basin	R_f ranges from 0 to 1. $R_f = 1$ denotes a circular basin	Horton (1945)
Elongation ratio (R_e)	$R_e = 1.128\sqrt{\frac{A}{L_b}}$ A: signifies the area of the basin, L_b: denotes the length of the basin	R_e is influenced by geology and climate. R_e varies from 0 to 1 (e.g. Wołosiewicz 2018). As the landscape evolves, the river basin becomes circular and Re tends to be 1	Schumm (1956)
Drainage texture (Dt)	$\mathrm{Dt} = \frac{\sum N_u}{P}$ ΣN_u: Total number of segments of all order in a basin, P: Perimeter of the basin	The lower values Dt indicate lower relief of basins, permeable lithology which has high infiltration capacity	Horton (1945)
Hypsometric integral (HI)	$\mathrm{HI} = \frac{\mathrm{Ele_{mean}} - \mathrm{Ele_{min}}}{\mathrm{Ele_{max}} - \mathrm{Ele_{min}}}$ Ele: Elevation	HI is an important index of basin development with respect to its erosional and depositional works	Pike and Wilson (1971)

4.2 *Geophysics*

The analytical expression of effect of gravity on uncompensated bathymetric (topographic) depths for a terrain is given by (Parker 1973):

$$g_{\mathrm{bathymetry}}(k) = 2\pi G(\rho_m - \rho_c)e^{-kd} \sum_{n=1}^{\infty} \frac{k^{n-1}}{n!} F\left\{h^n(x, y)\right\} \tag{1}$$

Here ρ_m and ρ_c are the densities of the mantle and the crust, respectively, in g cm^{-3}. The gravitational constant is indicated by G (m^3 kg^{-1} s^{-2}) and an undulating bathymetry Fourier transform by $F\{h(k)\}$. Further, d is the mean mantle depth (in km) and k the wave number in km^{-1}**.** Here n stands for the order of the equation. Putting $n = 1$ in Eq. (1), we get the first-order expression of the analytical solution (Watts 2001):

$$g_{\text{bathymetry}}(k) = 2\pi G(\rho_m - \rho_c)e^{-kd} F\{h(x, y)\} \tag{2}$$

After multiplying with an adjusting factor (σ) in right side, we can get $g_{\text{bathymetry}}$ value equivalent to f_{ag}.

$$g_{\text{bathymetry}}(k) = 2\sigma\pi G(\rho_m - \rho_c)e^{-kd} F\{h(x, y)\} \tag{3}$$

Equation (3) assumes that bathymetry (topography) is linearly connected with gravity anomaly in the wave number domain.

The percentage deviation (PD) between free-air gravity (FAG) (g_{fag}) and bathymetry gravity ($g_{\text{bathymetry}}$) has been estimated by using following formula (Eq. 9 of Dabbakuti and Ratnam 2017):

$$\text{PD} = \frac{g_{\text{bathymetry}} - g_{\text{fag}}}{g_{\text{bathymetry}}} \times 100 \tag{4}$$

The obtained PD values will show the comparison between FAG and modelled bathymetry gravity value.

5 Results

Three classes of watersheds with high, moderate and low tectonic activity have been obtained through AHP (Fig. 3). Three classes were also deduced based on IAT studied (Fig. 4).

The asymmetry factor (AF) is highest for SW1 (26.817), and the sub-watershed is tilted towards right. The value of AF is significantly high for the SW2 (20.710). SW6 portrays the minimum value of AF (5.587). SW7 and SW4 have lesser value of AF (6.816 and 7.410, respectively). The transverse topographic symmetry factor (T) represents the deviation of the main channel from its mid-path. It shows highest value (0.646) for SW7 followed by SW2 (0.620). SW5 marks the lowest value of T (0.146). The shape of basin is well-represented through the Elongation Ratio (R_e) and Form Factor (R_f). The value of R_e is lowest for SW1 (0.464). It is marked to be maximum (0.774) for SW3. SW5 and 6 have also higher values (0.745 and 0.727, respectively) for R_e. The value of R_f is lowest (0.169) for SW1. Lesser values of R_f are marked for SW2 (0.210) and SW4 (0.227). The maximum value (0.470) is marked for SW3. The drainage texture (Dt) is maximum (0.706) for SW5 and lowest (0.158) for SW7.

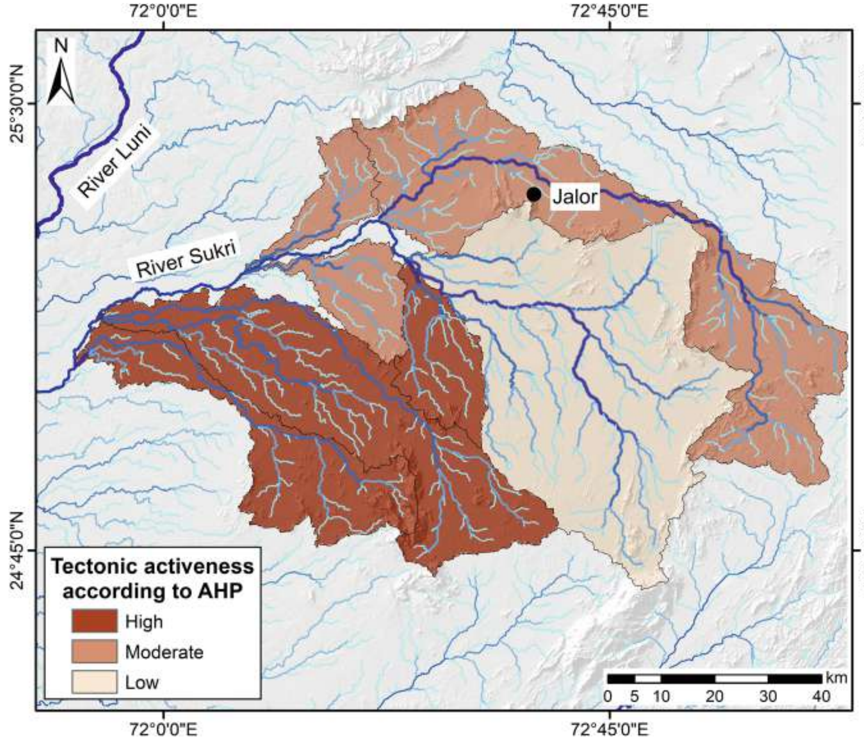

Fig. 3 Three classes—high, moderate and low—based on tectonic activeness as computed through Analytic Hierarchic Process (AHP)

The overall values of hypsometric integral (HI) is not very significant. It is maximum (0.209) for SW7 and minimum (0.083) for SW5.

Raster files are created for each parameter by applying the parameters at the sub-watershed scale. Weights are applied to every raster file by computing them using AHP (Table 2). The ArcGIS 10.4 platform's weighted sum approach has divided the sub-watersheds into three classifications based on the degree of tectonic activity: high, moderate and low. SW1, 2 and 4 are categorised as upper class. SW5, low class, and SW3, 6 and 7 are designated as mild.

Additionally, the sub-watersheds have been divided into three groups by the IAT: high, moderate and low (Table 3). SW4, SW6 and SW7 belong to the moderate class, whereas SW1 and SW2 are in the high class. The SW3 and SW5 are in the low class.

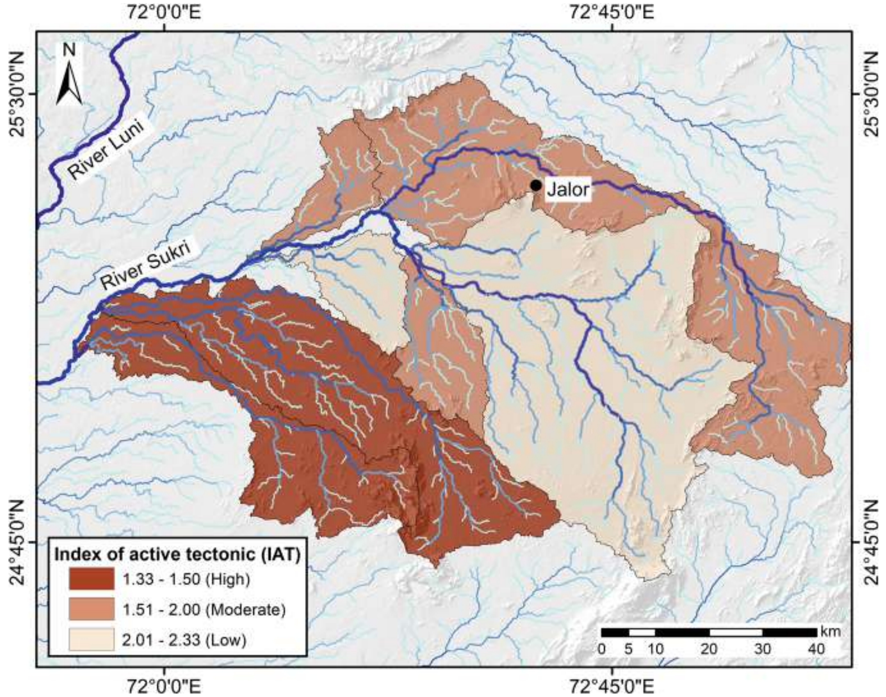

Fig. 4 Three classes—high, moderate and low—based on tectonic activeness of the sub-watersheds as computed with the help of Index of Active Tectonics (IAT)

6 Discussions

6.1 Geomorphology Perspective

The morphometric parameters show that the sub-watersheds have contrasting asymmetry as well as shape. The values of AF and T suggest that the sub-watersheds have different degree of tilting. Note that the overall slope of the land is from east to south-west. River Sukri has total six tributaries on its left hand and only one tributary on its right. Most of its sub-watersheds (SW1-3, 6) are tilted towards right depending presumably on the local gradient and lithological control. The shapes of the sub-watersheds as reflected through R_e and R_f suggest that SW1-2 and 6 are elongated. This further suggests the less lateral expansion of the sub-watersheds. Contrary to this, SW5 is more circular with more first- and second-order streams suggesting the lateral expansion of the sub-watershed. The drainage texture is also high for SW5 for this reason. The overall flat nature of the landscape, covered with Quaternary deposits, contributes to the lesser HI value of the sub-watersheds.

Interestingly, AHP- and IAT-based categorisation of the sub-watersheds provide near similar pattern of the tectonic activeness of the sub-watersheds. Both AHP and

Table 2 Weights calculated through the Analytic Hierarchic Process (AHP)

Parameter	Class	Class range	Weight
Asymmetry factor	1	15.245–26.817	31.57
	2	7.336–15.244	
	3	5.587–7.335	
Elongation ratio	1	0.464–0.644	25.19
	2	0.645–0.731	
	3	0.732–0.774	
Transverse topographic symmetry factor	1	0.450–0.646	19.28
	2	0.285–0.449	
	3	0.146–0.284	
Form factor	1	0.169–0.224	13.32
	2	0.225–0.416	
	3	0.417–0.470	
Drainage texture	1	0.359–0.706	6.16
	2	0.247–0.358	
	3	0.158–0.246	
Hypsometric integral	1	0.163–0.209	4.50
	2	0.112–0.162	
	3	0.083–0.111	

Table 3 Calculation for the Index of Active Tectonics (IAT)

Sub-watershed	HI	R_e	Dt	R_f	AF	T	Sum	IAT = Sum/n [n = number of parameters = 6]
1	2	1	3	1	1	1	9	1.5
2	2	1	2	1	1	1	8	1.33
3	2	3	3	3	1	2	14	2.33
4	3	1	2	2	2	2	12	2
5	2	3	1	3	2	3	14	2.33
6	1	2	1	2	3	2	11	1.83
7	1	1	3	2	3	1	11	1.83

IAT designate SW1 and 2 to be highly active tectonically. Similar confirmation was results are notices for SW6, 7 (moderately active tectonically) and SW5 (low tectonic activity).

6.2 Geophysical Perspective

The bathymetric (topographic) data has been accessed from General Bathymetric Chart of the Oceans (GEBCO) (Internet ref-1). The contour plot has been plotted using the MATBALB 2017b version, which includes seven watersheds (W) (Fig. 5). The results clearly show height variation within 200–1600 m with 1400 m upward continuation. No specific elevation trend is deciphered; however, several depressions were observed. For example, a major depression is displayed in the southern part of the Jalor district. This depression is > 300 m deep and ~ 20 km wide. The depression is filled up to a depth of ~ 85 m (Bajpai et al. 2001). The location of parallel and bifurcating channels of the Luni River together with laterally pinching sand bodies within this depression is possibly the result of tectonic activation in this zone leading to subsidence (Bajpai et al. 2001). The highest topography up to ~ 1600 m is found at the southern side of the W5 watershed and similar kinds of depressions are available surrounding it.

The gravity contour plot in the Sukri basin has been made using the MATLAB 2017b environment (Fig. 6). The study region includes seven watersheds (W), which show different gravity variations (Internet ref 2). Similar to the topographic map,

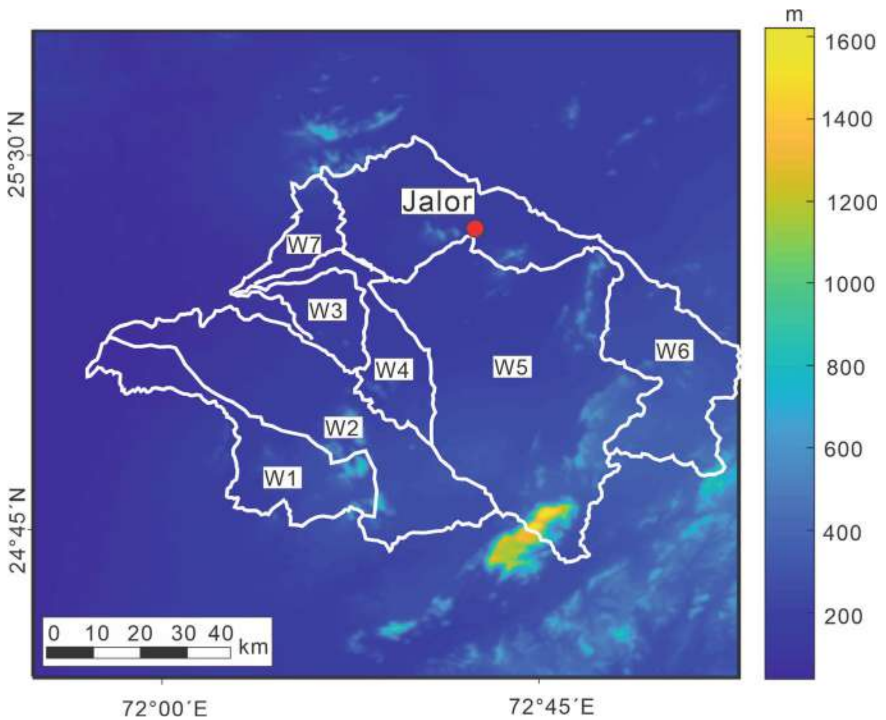

Fig. 5 The regional map of the Sukri basin with plot of bathymetry (elevation) data. Colour bar: height in m with respect to the mean sea level (MSL)

there is no particular trend available for gravity plots; however, it varies from −10 to 80 mGal in the entire region. The difference between high and low gravity anomalies is ~ 90 mGal, which cannot be explained based on the density difference between the basement material and alluvium, while it is possible because of grabens (Bajpai et al. 2001). The east and west parts of the region have the lowest gravity around −10 mGal. The gravity lows in the west and east are not simply due to the filling of low-density alluvium, rather these could be the results of a flexure or geologic fault (Parasnis 1966). A gravity depression up to -10 mGal exists in the western part of W2 and W3 watersheds possibly reflecting a graben structure. This graben extends towards the NE coinciding with the course of the Sukri River.

We selected $h(x, y)$ from the bathymetric height (GEBCO) and estimated the gravity effect of the uncompensated bathymetry. The densities of crust (ρ_c) and mantle (ρ_m) are taken as 2.67 g cm^{-3} and 3.3 g cm^{-3}, respectively (Ganguli and Pal 2023). In the current study, we selected d = 42 km and k = 0.04 km^{-1} (Ussami et al. 1993). The estimated gravity bathymetry plot has been shown in Fig. 7. As we can see from Eq. 3, that $h(x, y)$ multiplication coefficient is a constant value; hence, gravity bathymetry must follow the trend of bathymetry (the trend of Fig. 1) height, only the difference is that the results are in mGal unit. In the next step, we tried to understand the deviation between FAG gravity value and estimated bathymetry

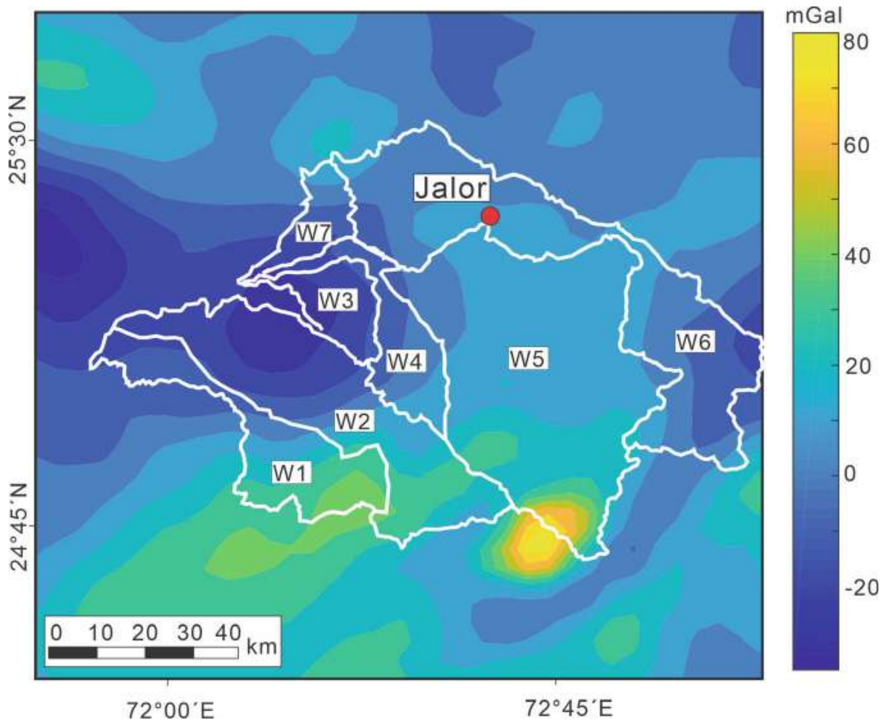

Fig. 6 Regional FAG map of the Sukri basin. Colour bar: gravity tend (mGal)

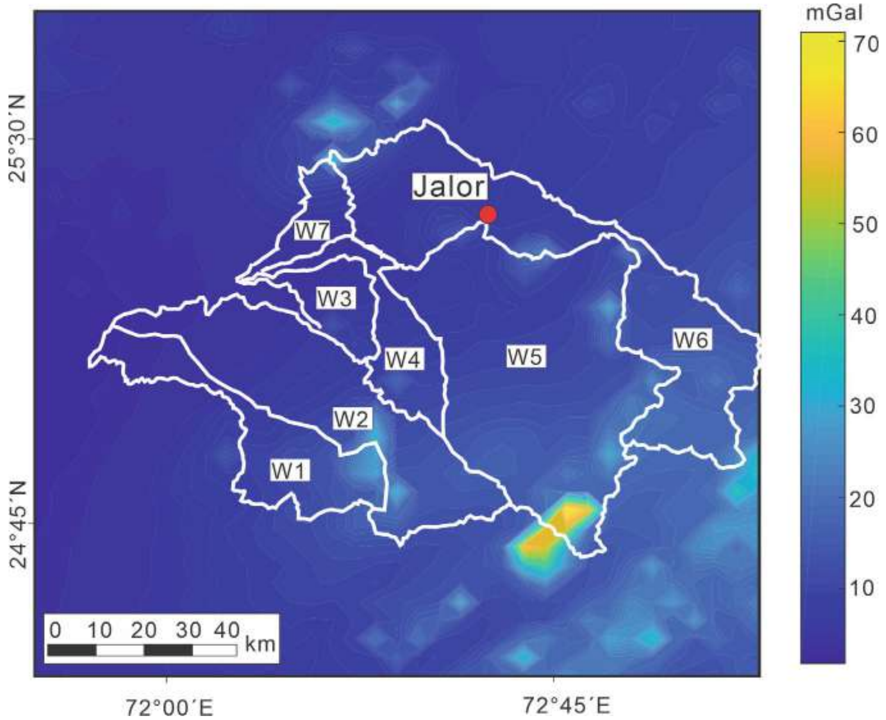

Fig. 7 Bathometry gravity plot (mGal) of the Sukri basin. Colour bar: gravity tend (mGal)

gravity values. We use Eq. 4 of percentage deviation (PD) and the obtained results are plotted in Fig. 8. Here positive deviation indicates that bathymetry gravity values are high. In contrast, negative values indicate they are low. The value of this deviation varies from −400 to 1200% within the region.

7 Conclusions

Based on AHP and IAT studies, sub-watershed 1 (SW1) and 2 delineated for the Sukri River are highly active tectonically. SW6 and 7 are moderately active, and SW5 shows a low tectonic activeness.

The bathymetric (topographic) results in the Sukri basin show height variation within 200–1600 m, while the gravity results have variation from −10 to 80 mGal. Both bathymetry (topographic) and gravity plots have no trend in the entire region. The difference between high and low gravity anomalies is ~ 90 mGal, which is possible because of grabens. A gravity depression up to −10 mGal exists in the western part of W2 and W3 watersheds possibly reflecting a graben structure. The deviation between FAG gravity value and estimated bathymetry (topographic) gravity

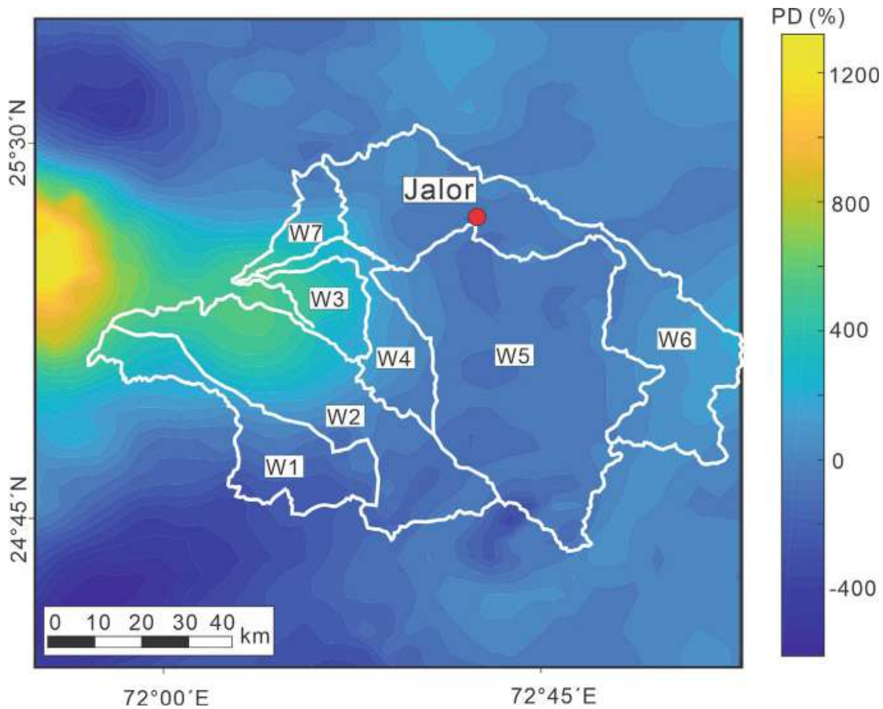

Fig. 8 The percentage deviation between bathymetry gravity and FAG in the Sukri basin

values is studied. The positive deviation (1200%) indicates that bathymetry (topographic) gravity values are high and in contrast, the negative deviation (−400%) connotes that they are low in the Sukri basin.

Acknowledgements A self-funded work. Springer is thanked for proofreading and publishing. Mukherjee and Kar (2025) summarized this article.

Abbreviations and Symbols

AF	Asymmetry Factor
AHP	Analytic Hierarchic Process
D_t	Drainage texture
$F\{h(k)\}$	Fourier transform
FAG	Free-air gravity
G	Gravitational constant
GEBCO	General Bathymetric Chart of the Oceans
HI	Hypsometric integral
$h(x, y)$	Bathymetric height

IAT	Index of Active Tectonics
MSL	Mean Sea Level
PD	Percentage Deviation
R_e	Elongation ratio
R_f	Form Factor
SRTM	Shuttle Radar Topographic Mission
T	Transverse Topographic Symmetry
ρ_c	Density of crust
ρ_m	Density of mantle

References

Anand, A.K., and S.P. Pradhan. 2019. Assessment of active tectonics from geomorphic indices and morphometric parameters in part of Ganga basin. *Journal of Mountain Science* 16: 1943–1961.

Benyas, K., A. Aarab, A. Qarbous, A. Lakhloufi, A. Manar, M. Amar, A. Idrissi, and M. Elmimouni. 2021. Exploiting aeromagnetic and gravity data interpretation to delineate massif deposits of Rehamna Area (Western Meseta-Morocco). *The Iraqi Geological Journal* 54: 13–28.

Bajpai, V.N., T.S. Roy, and S.K. Tandon. 2001. Subsurface sediment accumulation patterns and their relationships with tectonic lineaments in the semi-arid Luni river basin, Rajasthan, Western India. *Journal of Arid Environments* 48: 603–621.

Biswas, M., M.P. Gogoi, B. Mondal, T. Sivasankar, S. Mukherjee, and S. Dasgupta. 2022a. Geomorphic assessment of active tectonics in Jaisalmer basin (western Rajasthan, India). *Geocarto International* 37: 12382–12413.

Biswas, M., M.K. Puniya, M.P. Gogoi, S. Dasgupta, S. Mukherjee, and N.R. Kar. 2022b. Morphotectonic analysis of petroliferous Barmer rift basin (Rajasthan, India). *Journal of Earth System Science* 131: 140.

Biswas, M., A. Raha, S. Mukherjee, and V.S. Kotak. 2024. Geomorphic imprints of active tectonics of the Bikaner-Nagaur petroliferous rift basin and its surroundings (western Rajasthan, India). *Journal of the Geological Society of India* 100: 377–390.

Brookfield, M.E. 1998. The evolution of the great river systems of southern Asia during the Cenozoic India-Asia collision: Rivers draining outhwards. *Geomorphology* 22: 285–312.

Chen, Z. 2003. Geoscientific thinking of Dujiangyan water-conservancy system [in Chinese]. *Quaternary Science Reviews* 23: 211–217.

Cox, R.T. 1994. Analysis of drainage-basin symmetry as a rapid technique to identify areas of possible Quaternary tilt-block tectonics: An example from the Mississippi Embayment. *Geological Society of America Bulletin* 106: 571–581.

Dabbakuti, J.K., and D.V. Ratnam. 2017. Modeling and analysis of GPS-TEC low latitude climatology during the 24th solar cycle using empirical orthogonal functions. *Advances in Space Research* 60: 1751–1764.

Dasgupta, S., & Mukherjee, S. (2017). Brittle shear tectonics in a narrow continental rift: Asymmetric nonvolcanic Barmer Basin (Rajasthan, India). *The Journal of Geology*, 125(5): 561–591.

Dewanto, B.G., R. Priadi, L.S. Heliani, A.S. Natul, M. Yanis, I. Suhendro, and A.M. Julius. 2022. The 2022 Mw 6.1 Pasaman Barat, Indonesia Earthquake, confirmed the existence of the Talamau segment fault based on teleseismic and satellite gravity data. *Quaternary* 5: 45.

El Hamdouni, R., C. Irigaray, T. Fernández, J. Chacón, and E.A. Keller. 2008. Assessment of relative active tectonics, southwest border of the Sierra Nevada (southern Spain). *Geomorphology* 96: 150–173.

Ganguli, S.S., and S.K. Pal. 2023. Gravity-magnetic appraisal of the southern part of Cauvery Basin, Eastern Continental Margin of India (ECMI); An evidence of volcanic rifted margin. *Frontiers in Earth Science* 11: 1190106.

Gao, M., G. Zeilinger, X. Xu, Q. Wang, and M. Hao. 2013. DEM and GIS analysis of geomorphic indices for evaluating recent uplift of the northeastern margin of the Tibetan Plateau, China. *Geomorphology* 190: 61–72.

Goorabi, A., and A. Nohegar. 2005. Geomorphological evidence of active tectonic of Darake catchment. *Journal of Natural Geographical Studies* 60: 96–177.

Hare, P.W., and T.W. Gardner. 1985. Geomorphic indicators of vertical neotectonism along converging plate margins, Nicoya Peninsula, Costa Rica. *Binghamton Symposia in Geomorphology: International Series* 15: 75–104.

Horton, R.E. 1945. Erosional development of streams and their drainage basins: Hydrophysical approach to quantitative morphology. *GSA Bulletin* 56: 275–370.

Internet ref 1. https://download.gebco.net/. Accessed on 12 Dec 2023.

Internet ref-2. https://bgi.obs-mip.fr/data-products/outils/egm2008-anomaly-maps-visualization/. Accessed on 13 July 2023.

Kar, N.K., D. Mani, S. Mukherjee, S. Dasgupta, M.K. Puniya, A.K. Kaushik, M. Biswas, and E.V.S.S.K. Babu. 2022. Source rock properties and kerogen decomposition kinetics of Eocene shales from petroliferous Barmer basin, western Rajasthan, India. *Journal of Natural Gas Science and Engineering* 100: 104497.

Kar, N.R., D. Mani, B.S. Seetha, E.V.S.S.K. Babu, S. Mukherjee, S. Dasgupta, M.K.R. Mudiam. In Press. Organic provenance and depositional environment of Eocene carbonaceous rocks from petroliferous Barmer basin, Western Rajasthan, India. *Journal of the Geological Society of India.*

Keller, E.A., Pinter, N., 2002. Active tectonics: Earthquakes, uplift, and landscape. Prentice Hall.

Kirby, E., and K.X. Whipple. 2012. Expression of active tectonics in erosional landscapes. *Journal of Structural Geology* 44: 54–75.

Malik, M., M. Bhat, and N.A. Kuchay. 2011. Watershed based drainage morphometric analysis of Lidder catchment in Kashmir valley using Geographical Information System. *Recent Research in Science and Technology* 3: 118–126.

Mukherjee, S., and N.R. Kar. 2025. Introduction to *Geosciences of the Rajasthan basins, India.* Springer. pp. v–viii. Singapore: Springer. ISBN 978-981-96-3004-2.

Nyalugwe, V.N., M.G. Abdelsalam, A. Katumwehe, K.L. Mickus, and E.A. Atekwana. 2020. Structure and tectonic setting of the Chingale Igneous Ring Complex, Malawi from aeromagnetic and satellite gravity data: Implication for Precambrian terranes collision and Neogene-Quaternary rifting. *Journal of African Earth Sciences* 163: 103760.

Okumura, M., and A.G. Araujo. 2014. Long-term cultural stability in hunter–gatherers: A case study using traditional and geometric morphometric analysis of lithic stemmed bifacial points from Southern Brazil. *Journal of Archaeological Science* 45: 59–71.

Parasnis, D.S. 1966. *Mining geophysics*, 395. Amsterdam: Elsevier.

Parker, R.L. 1973. The rapid calculation of potential anomalies. *Geophysical Journal International* 31: 447–455.

Pike, R.J., and S.E. Wilson. 1971. Elevation relief ratio, hypsometric integral and geomorphic area-altitude analysis. *GSA Bulletin* 82: 1079–1084.

Puniya, M.K., A.K. Kaushik, S. Mukherjee**,** S. Dasgupta, N.K. Kar, M. Biswas, R. Choudhary. 2023a. New structural geological input from the Barmer Basin, Rajasthan (India). In *Structural geology and tectonics field guidebook—Volume 2*, ed. S. Mukherjee, 285–296. Springer Geology.

Puniya, M.K., A.K. Kaushik, S. Mukherjee, N.R. Kar, M. Biswas, R. Choudhury. 2023b. Structural geology and stability issue of the Giral Lignite Mine, Rajasthan, India. In *Structural geology and tectonics field guidebook—Volume 2*, ed. S. Mukherjee, 297–310. Springer Geology.

Rodrigo-Comino, J., T. Iserloh, T. Lassu, A. Cerdà, S.D. Keestra, M. Prosdocimi, C. Brings, M. Marzen, M.C. Ramos, J.M. Senciales, J.D. Ruiz Sinoga, M. Seeger, and J.B. Ries. 2016. Quantitative comparison of initial soil erosion processes and runoff generation in Spanish and German vineyards. *Science of the Total Environment* 565: 1165–1174.

Surya, R.A., F. Abdullah, D. Darisma, M. Yanis, and N. Ismail. 2019. Sedimentation process in Kuala Gigieng Coast, Aceh Besar based on magnetic and gravity surveys. *IOP Conference Series: Earth and Environmental Science* 348 (1): 012040.

Schumm, S.A. 1956. Evolution of drainage systems and slopes in badlands at Perth Amboy, New Jersey. *Bulletin of Geological Society of America* 67: 597–646.

Telvari, A. 2009. *Preliminaries of engineering and organizing rivers*, 454p. Agricultural Ministry of Iran: Abkhiz publication.

Watts, A.B. 2001. *Isostasy and flexure of the lithosphere*. Cambridge University Press.

Wołosiewicz, B., 2018. The influence of the deep seated geological structures on the landscape morphology of the Dunajec River catchment area, Central Carpathians, Poland and Slovakia. Geoscience Journal 7: 21–47.

Yanis, M., A. Faisal, A. Yenny, Z. Muzakir, M. Abubakar, and I. Nazli. 2020. Continuity of great sumatran fault in the marine area revealed by 3D inversion of gravity data. *Jurnal Teknologi* 83: 145–155.

Yanis, M., A.V. Simanjuntak, F. Abdullah, M. Marwan, and A.A. Ghani. 2023. Application of seismicity and gravity observation-based filtering model for mapping a fault structure in Weh Island, Indonesia. *The Iraqi Geological Journal* 56: 260–274.

Yemani, M., M. Alaei-Talghani, and S. Shahbazi. 2011. Morphotectonic and its effect on bed changes and pattern of Gharehsu river. *Journal of Geography and Regional Development* 17: 125–143.